Environmental Science & Technology

Article

pubs.acs.org/est

A 2.5D Reactive Transport Model for Fracture Alteration Simulation

Hang Deng,*[,†] Sergi Molins,[†] Carl Steefel,[†] Donald DePaolo,[†,‡] Marco Voltolini,[†] Li Yang,[†] and Jonathan Ajo-Franklin[†]

[†]Lawrence Berkeley National Laboratory, Berkeley, California 94720, United States

[‡]Earth and Planetary Science, University of California, Berkeley, Berkeley, California 94720, United States

Supporting Information

ABSTRACT: Understanding fracture alteration resulting from geochemical reactions is critical in predicting fluid migration in the subsurface and is relevant to multiple environmental challenges. Here, we present a novel 2.5D continuum reactive transport model that captures and predicts the spatial pattern of fracture aperture change and the development of an altered layer in the near-fracture region. The model considers permeability heterogeneity in the fracture plane and updates fracture apertures and flow fields based on local reactions. It tracks the reaction front of each mineral phase and calculates the thickness of the altered layer. Given this treatment, the model is able to account for the diffusion limitation on reaction rates associated with the altered layer. The model results are in good agreement with an experimental study in which a CO_2-acidified brine was injected into a fracture in the Duperow Dolomite, causing dissolution of calcite and dolomite that result in the formation of a preferential flow channel and an altered layer. With an effective diffusion coefficient consistent with the experimentally observed porosity of the altered layer, the model captures the progressive decrease in the dissolution rate of the fast-reacting mineral in the altered layer.

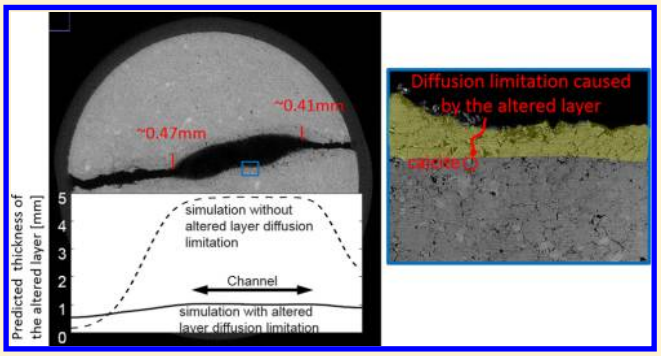

1. INTRODUCTION

Fractures are important flow pathways in subsurface environments, particularly in formations with relatively low permeability, such as the caprock for geological carbon-storage reservoirs, waste repositories, and shale gas plays.[1−4] Fractures dominate fluid migration and solute transport in these systems and are subject to alteration caused by water−rock interaction.[5−12] Understanding the dynamic evolution of fractures is key to the accurate assessment of the performance of such systems.

Previous experimental studies have shown two types of complex geometrical changes in fractures after being exposed to reactive fluid flow. One is the enlargement or reduction of the fracture apertures resulting from dissolution or precipitation in the fractures.[6−13] The spatial patterns of such changes are largely controlled by flow regimes, typically characterized by the Damköhler number (Da).[9,14] However, when minerals of different reactivity are present, a single Da number cannot be used to accurately describe the system, and aperture change is instead dominated by the spatial patterns of the reactive minerals. Specifically, if the reactive phase is dispersed in the rock matrix, preferential dissolution of the fast-reacting mineral results in another type of fracture alteration, i.e., the formation of a porous altered layer in the near-fracture region.[5,6,15]

In response to the geometric alteration of the fracture, permeability evolves over time. For example, fracture aperture enlargement, especially channelization, can cause substantial fracture-permeability enhancement.[8] The extent of the increase, however, may be mitigated by the presence of nonreactive mineral bands and the development of an altered layer.[16] In addition, the alteration of fracture geometry can cause solute transport and subsequent geochemical reactions in the fracture to change. Channeling has been reported to reduce the global reaction rate by limiting the accessibility of nonchannelized fracture surfaces to fresh reactive fluid.[8] The overall reaction rate has also been observed to decrease exponentially as an altered layer develops on the fracture surfaces[5,15] because the altered layer serves as a diffusion barrier that reduces mass transfer between the fracture and rock matrix.[5] Despite these observations, there is still a lack of predictive understanding of the development of the altered layer and its influence on the subsequent evolution of the fracture.[5]

To improve our fundamental understanding of fracture alteration and to develop predictive capabilities, it is critical to capture the feedback between fluid flow and geochemical reactions. In this regard, reactive transport modeling provides an indispensable investigative tool.[17] A series of reactive

Received: May 2, 2016
Revised: June 27, 2016
Accepted: June 30, 2016

DOI: 10.1021/acs.est.6b02184
Environ. Sci. Technol. XXXX, XXX, XXX−XXX

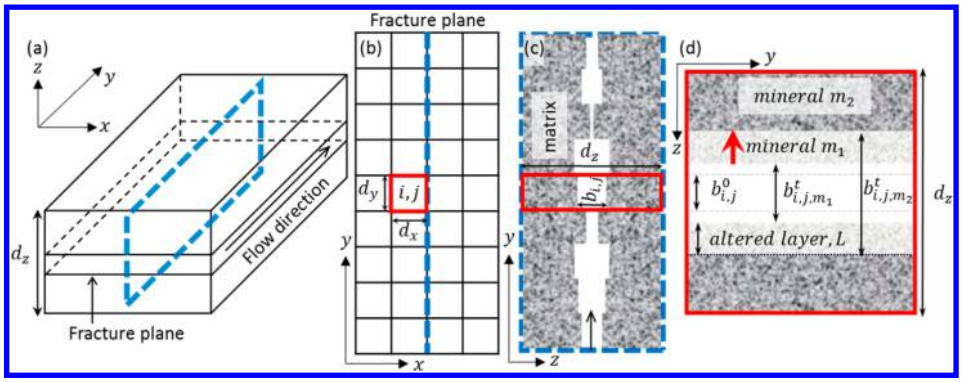

Figure 1. Schematic illustration of the 2.5D continuum model. (a) A 3D schematic of the fractured domain, (b) a 2D mesh discretized along the fracture plane, (c) conceptual representation of the cross-section along the flow direction and across the fracture aperture (highlighted by the blue dashed box in (a) and by the blue dashed line in (b)), and (d) a conceptual graph of the continuum representation within each grid cell (highlighted by the red boxes in (b) and (c)) in the presence of binary minerals with different reactivity.

transport models, with variable complexity and computational sophistication, have been proposed to investigate fracture alteration. For example, a 1D model was used to simulate reactions in the rock matrix along the direction perpendicular to the fracture plane[18] and showed that diffusion and reaction in the rock matrix can strongly affect fluxes from the altered layer to the fracture.[19] Although 1D models are in general computationally efficient and can provide important insights, they do not capture the topography of the fracture plane and cannot simulate processes that are inherently two-dimensional, such as channelization.[8,20] Instead, 2D reactive transport models have been used to capture the spatial patterns of fracture alteration in the fracture plane.[9,21] For example, the model developed by Yasuhara and Elsworth[21] captures the competing processes of pressure solution and free-face dissolution in the fracture and was used to investigate fracture aperture, contact area and permeability evolution resulting from these processes under different effective stresses and flow rates.

Existing 2D fracture-plane reactive transport models focus on the processes at the fracture surface; they do not account for mass transfer between the fracture and the rock matrix and, thus, the impacts of the porous altered layer in the near-fracture regions. Although models that simulate the 2D cross-section along the flow direction and perpendicular to the fracture plane capture the effects of the altered layer on geochemical reactions, they neglect the spatial variation in the fracture plane that determines fracture permeability.[18,22] Moreover, fracture topology largely affects the local flow and stress that determine the likelihood of particle mobilization and the possibility of clogging in the fracture.[5,6] 3D models may be used to capture both the spatial variation in the fracture plane and the mass transfer between the rock matrix and the fracture. However, 3D representations of fractures, with relatively small apertures compared to fracture-plane dimensions, typically require fine meshing, resulting in a large number of grid cells and prohibitive computational costs. As a result, the application of 3D reactive transport models to discrete fractures is rare.

In this study, our objective is to bridge the gap between the 2D and 3D reactive transport models. For this purpose, we introduce a 2.5D model that is computationally efficient and captures the processes across the fracture aperture that are important to fracture alteration. Specifically, the model captures the development and the impacts of the altered layer in the near-fracture region while allowing the simulation of the spatial patterns of fracture geometric alteration. We organize the manuscript in the following manner. First, the model framework and its novel features are detailed in the Methods section. Second, simulation results are presented to demonstrate the performance of the model. For this purpose, data from a fracture-flow experiment involving the injection of high pCO_2 brine into the Duperow Dolomite, which resulted in the formation of a preferential channel and the development of an altered layer, were used in the model simulations and for comparison. We conclude the paper with a discussion of the implications and potential applications of this model.

2. MATERIALS AND METHODS

2.1. 2.5D Continuum Model. The 2.5D continuum model is implemented by modifying the reactive transport code CrunchFlow[23] and is depicted conceptually in Figure 1. The fractured domain is discretized in two dimensions parallel to the fracture plane. Each grid cell is represented as a continuum, i.e., it consists of a combination of fracture and rock matrix. The physical properties of each grid cell are calculated based on the local fracture aperture ($b_{i,j}$) and vary within the fracture plane. It should be noted that instead of the Kozeny−Carman relationship commonly used in continuum models, the permeability ($k_{i,j}$) is calculated and updated based on the cubic law developed for fractures.[18,24−26]

$$k_{i,j} = b_{i,j}^3/12d_z \quad (1)$$

In this equation, d_z is the thickness of the simulated domain in the third dimension perpendicular to the fracture plane. Note that because all physical properties are normalized against d_z, its choice does not affect the simulation results as long as no mineral is depleted within the given simulation time.

Although the dimension across the fracture aperture is not resolved explicitly, and no transverse flow is considered, the 2.5D model includes two new features that allow the consideration of some processes in this dimension. First, instead of having a single aperture value for each grid cell and updating it on the basis of porosity change, the aperture of each mineral phase (b_{i,j,m_n}) is calculated from the volume percent of that mineral measured for the intact rock matrix (f_{i,j,m_n}) and the volume fraction of the mineral in the grid (V_{i,j,m_n}) (eq 2). In this case, the mineral fronts start at the same locations but propagate at different rates according to the reaction rate of the respective mineral phase. In the approach used here, permeability is updated according to the position of the

DOI: 10.1021/acs.est.6b02184
Environ. Sci. Technol. XXXX, XXX, XXX−XXX

mineral-phase front that moves the slowest (eq 3). In other words, the porous layer of this mineral phase, left behind by dissolution of the fast-reacting mineral(s), is assumed to be hydraulically impermeable like the initial unaltered rock matrix. This is a valid approximation as long as the fracture permeability is significantly larger than the altered rock-matrix permeability. Previous experimental and modeling work has shown that the altered layer has negligible contribution to fracture permeability.[5,22]

$$b_{i,j,m_n} = d_z\left(1 - \frac{V_{i,j,m_n}}{f_{i,j,m_n}}\right) \tag{2}$$

$$b_{i,j} = \min\{b_{i,j,m_1}, ..., b_{i,j,m_n}\} \tag{3}$$

The second new feature of the 2.5D model is that the thickness of the altered layer is tracked so that the diffusion limitation resulting from the presence of the altered layer can be accounted for. The thickness of the altered layer (L) is calculated as the difference between the apertures of the fast-reacting mineral phase (m_2 in Figure 1d) and the remaining mineral phase (m_1 in Figure 1d).

As the altered layer develops, the reaction of the fast-reacting mineral phase is increasingly limited by the diffusive transport of the reaction products through the porous altered layer away from the mineral surface and toward the fracture. The diffusion controlled reaction rate (R_{diff}) is calculated to account for this diffusion limitation imposed by the altered layer (eq 4). The diffusion controlled rate constant (k_{diff}) is calculated using the formulation (eq 5) that is widely applied for systems that are dominated by microscale transport processes of reactants or products through a diffusion boundary layer or porous altered layer.[26−32] In the case of a porous altered layer, the effective diffusion coefficient of the porous media (D_{eff}) used depends on the porosity (ϕ) and tortuosity of the material. It differs from the free-phase molecular diffusion coefficient (D_0) that is used for the calculation of lateral diffusion in the fracture plane. The deviation can be quantified by the formation factor F (eq 6), which is based on Archie's law (eq 7) and is a function of porosity.[33] In the power-law relationship, a is an empirical parameter, and m is the cementation exponent.

$$R_{diff} = -k_{diff}A(C_{eq} - C_{bulk}) \tag{4}$$

$$k_{diff} = \frac{D_{eff}}{L} \tag{5}$$

$$D_{eff} = \frac{D_0}{F} \tag{6}$$

$$F = a\phi^{-m} \tag{7}$$

Because the flux of reactants to the mineral surface must equal the surface reaction rate, for a mineral subject to a mixed kinetic control, the effective reaction rate coefficient can be derived analytically (eq 8).[29] It follows that the effective reaction rate (R_{eff}) is a function of R_{diff} (which assumes that the rate is fully controlled by diffusion in the porous boundary layer adjacent to the fracture) and the surface-reaction controlled rate (R_{surf}, which assumes that there is no boundary layer and that the rate is determined by solute concentrations in the fracture fluid) (eq 9). Accordingly, R_{diff} is evaluated using the difference between the equilibrium concentration and the bulk concentration in the fracture of the species that dictates the mineral reaction instead of using the actual concentration gradient across the altered layer. The surface area that the diffusive flux crosses (A) is equal to the projected fracture surface area within the grid.

$$k_{eff} = \frac{1}{\frac{1}{k_{diff}} + \frac{1}{k_{surf}}} \tag{8}$$

$$R_{eff} = -k_{eff}A(C_{eq} - C_{bulk}) = \frac{1}{\frac{1}{-k_{diff}A(C_{eq} - C_{bulk})} + \frac{1}{-k_{surf}A(C_{eq} - C_{bulk})}} = \frac{1}{\frac{1}{R_{diff}} + \frac{1}{R_{surf}}} \tag{9}$$

$$R_{surf} = -k_{surf}A_{rxn}\left(1 - \frac{IAP}{K_{eq}}\right) \tag{10}$$

Although eq 8 assumes first-order kinetics, here, we expand its application in eq 9 by including a surface reaction rate based on the transition-state theory (eq 10), where k_{surf} refers to the kinetic coefficient, A_{rxn} denotes the reactive surface area, and the term in the parentheses with the ionic activity product (IAP) and the solubility constant (K_{eq}) of the mineral describes the chemical affinity or departure from equilibrium of the fracture fluid. This formulation allows us to consider mineral reactions with a more complex dependence on aqueous species, e.g., dependence of calcite dissolution on H^+.[34]

The formulation of eq 9 ensures that the lower rate always dominates, which makes sense in the case where the reaction mechanisms are in parallel, and it provides a continuous transition between the surface-reaction controlled rate and the diffusion controlled rate.

2.2. Duperow Fracture-Flow Experiment. For the development and testing of the model, data from a high-pressure fracture reactive flow experiment were used. The experimental study is detailed in Ajo-Franklin et al. (2016),[15] and therefore, only a brief summary is included here to provide information that is critical for the current modeling investigation. In the experiment, a fractured core 2.54 cm long and 0.95 cm in diameter was subjected to constant flow of CO_2-acidfied brine for 113 h under high pressure (pore pressure 96.5 bar) at room temperature. The influent was prepared by equilibrating DI water with CO_2 at 35 bar at 25 °C, and the measured amount of CO_2 dissolved in the solution was used to calculate the total carbon concentration (1.2 mol/kgw). The core is from the Devonian age Duperow formation, and an X-ray powder diffraction measurement on a similar sample gave the following composition: dolomite (86.9 wt %), calcite (9.5 wt %), plagioclase (1.8 wt %), smectite clay (1.8 wt %), and quartz (<1 wt %). In situ micro-CT images of the fractured core were collected at different stages of the experiment at Beamline 8.3.2 of the Advanced Light Source (LBNL) as well as higher-resolution tomography images of post-reaction subsamples. Key results from the experimental effort include (1) localized fracture-aperture enlargement, (2) development of a porous altered layer due to rapid calcite dissolution, and (3) an increase in the dolomite dissolution rate as the experiment evolved. Secondary results included fracture surface roughening as well as small amounts of fine-particle mobilization, processes not addressed in this study.

For the purpose of the simulation, several simplifications were made. First, the aperture map derived from the micro-CT images of the fracture before reaction with a resolution of 6.75

DOI: 10.1021/acs.est.6b02184
Environ. Sci. Technol. XXXX, XXX, XXX−XXX

μm is down-sampled to generate a 2D mesh with a grid size of 54 μm. d_z used in the simulation is 1 cm, consistent with the diameter of the core. Second, only two minerals, dolomite and calcite, are included, and the other minerals present are treated as dolomite. This simplification is justified by the small weight fractions of these minerals and the extremely low concentrations of cations other than Ca and Mg in the effluent measurements. Third, the mineral composition is assumed to be spatially homogeneous. Visual inspection of the micro-CT images confirmed that the rock sample used in the flow experiment is homogeneous except for some sporadic calcite-rich veins, and examinations of the reacted fracture showed no evident impacts of these veins on fracture evolution.

Analysis of the high-resolution tomography images revealed that the intact rock matrix has an average porosity of 10% (see Supporting Information). Based on the measured weight fractions and the average porosity, we calculated the volume fractions of dolomite and calcite used in the simulations as 81% and 9%, respectively. The reactive surface area of each mineral is scaled based on the respective volume fraction.

The calculation of k_{surf} incorporates the pH dependence (and the dependence on the activity of total dissolved CO_2, $a_{H_2CO_3^*}$) of the respective dissolution reaction. The parameters used for calcite and dolomite follow Deng et al. (2015)[8] and Pokrovsky et al. (2005),[35] respectively (see Table S1).

$$k_{surf,calcite} = k_1 a_{H^+} + k_2 a_{H_2CO_3^*} + k_3 \quad (11)$$

$$k_{surf,dolomite} = k_4 a_{H^+}^{0.5} \quad (12)$$

Initially, the fracture is filled with DI water. At the inlet, the influent, following the experiment, is injected into the fracture at a constant rate (5 μL/min) and is equally distributed among the center one-fifth of the grids, where the injection tube is located. At the outlet, a constant pressure is maintained. The two boundaries parallel to the flow direction allow no flux or mass transfer. D_0 is assumed to be the same for all species, and a value of 1.0×10^{-9} m^2/s at 25 °C was used in the simulations.[28] D_{eff} is less well-constrained for the altered layer and will be discussed in more detail in the following section.

In each grid, the total mineral surface area is calculated by multiplying the geometrical fracture surface area ($2d_xd_y$) with a surface roughness factor (SRF). SRF is an empirical parameter used to account for the difference between the geometrical surface area and the true surface area, which because of surface roughness is often larger. In this study, a SRF of four is used so that the simulated effluent concentrations are consistent with the effluent measurements taken at the early stage of the experiment before the altered layer has formed.

More details about the geochemical properties and numerical schemes used in the simulations are provided in the Supporting Information.

3. RESULTS AND DISCUSSION

We first compare the simulation results from the 2.5D continuum model with the experimental observations. To demonstrate the impacts of the altered layer on solute transport and subsequent geochemical reactions, we included comparative simulations with and without the diffusion limitation imposed by the altered layer on the fast-reacting mineral, calcite in this case. Simulations without the diffusion limitation update the reaction term using R_{surf}, whereas simulations with the diffusion limitation use R_{eff} instead. We also explore the broader application of the model at the end of this section.

3.1. Effective Diffusion Coefficient. In the diffusion limitation configuration, the thickness of the altered layer is endogenous, and the only exogenous variable is D_{eff}. For a given porosity, D_{eff} can be calculated using eqs 6 and 7. The parameters a and m are typically determined by fitting the formation-resistivity factor and the porosity data of a sample with a power-law curve and are highly variable depending on the petrophysical properties of the rock. For carbonate rocks, a and m were reported to be between 0.23 and 1.78 and between 1.64 and 2.86, respectively.[36] Given the reported a and m ranges, D_{eff} is estimated to be approximately 0.4×10^{-10} m^2/s for a porosity of 19%. Using a porosity of 19% for the altered layer is consistent with the simplified modeling system, in which the initial porosity of the rock matrix is 10% and the volume fraction of calcite is 9%. However, if D_{eff} is set to be 0.4×10^{-10} m^2/s, the simulated effluent Ca concentration is considerably lower than the experimental data, showing a steeper decreasing trend (Figure 2).

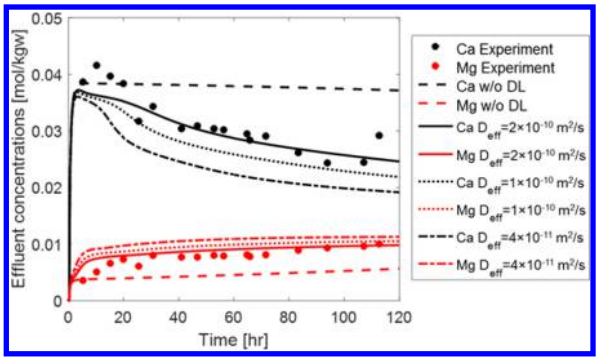

Figure 2. Effluent Ca (black) and Mg (red) concentrations measured in the experiment (●) and predicted by the simulations. The dashed lines (--) plot shows results of the simulation without the diffusion limitation of the altered layer. The predicted effluent chemistries from the simulations with the diffusion limitation are plotted in solid lines (—) for $D_{eff} = 2 \times 10^{-10}$ m^2/s, dotted lines (···) for $D_{eff} = 1 \times 10^{-10}$ m^2/s, and dash–dot lines (-·) for $D_{eff} = 0.4 \times 10^{-10}$ m^2/s.

There are two possible explanations for the aforementioned discrepancy. First, as revealed by the high-resolution tomography images of the postreaction subsamples, the porosity of the altered layer is higher than 19%. The porosity can reach 36% close to the fracture surface, and the average porosity is approximately 29%. The higher porosity may be a result of the fact that calcite is the cementing material, and its dissolution can change the structure of the rock matrix and cause particle detachment. The high porosity of the altered layer may also indicate some dissolution of dolomite in the altered layer. For a porosity of 29% as observed in the images, the estimated D_{eff} ranges from 0.7×10^{-10} to 1.3×10^{-10} m^2/s. Using a value of 1.0×10^{-10} m^2/s, the model predicts effluent Ca concentrations that are only slightly lower than the experimental observation. The remaining difference may be attributed to the fact that calcite is not uniformly dispersed in the rock matrix as assumed and instead is locally clustered as illustrated in the micro-CT images. Consequently, the dissolution of calcite can leave behind large pores or vugs in the altered layer. Because the pore structure is less-tortuous in such large pores, D_{eff} is expected to be high. The a and m values reported in the literature may fail

DOI: 10.1021/acs.est.6b02184
Environ. Sci. Technol. XXXX, XXX, XXX−XXX

to capture these features, given that the determination of a and m are highly specific to the samples that are used.

Based on the experimental solute-concentration measurements, we estimated the value of D_{eff} as 2×10^{-10} m^2/s, which is reasonable given the measured porosity. In the rest of the section, the reported simulation with the diffusion limitation of the altered layer uses this D_{eff} value.

It should be noted that although the effluent chemistry and, thus, the magnitudes of the aperture increase and the thickness of the altered layer are affected by the value of D_{eff} used in the modeling, the spatial patterns of the aperture increase and the altered layer are not sensitive to it (see the Supporting Information).

3.2. Effluent Chemistry. In the early stage of the experiment, the measured Ca concentration was approximately 0.037 mol/kgw and is close to equilibrium with respect to calcite. The Ca concentration decreased to ~0.025 mol/kgw at the end of the experiment. In the simulations, after the reactive fluid pushes the initial DI water out of the fracture, the reaction rate of calcite is at its highest, resulting in a Ca concentration of ~0.037 mol/kgw. If a diffusion limitation from the altered layer is not included in the modeling, the simulated Ca concentration remains almost constant. In contrast, with the diffusion limitation included, the simulated Ca concentration captures the temporal trend observed in the experiment, decreasing from 0.037 to 0.025 mol/kgw by the end of the simulation period. This decrease reflects the reduction of the calcite dissolution rate caused by the altered layer. As the altered layer grows, R_{diff} decreases progressively (eq 4). In grid cells where R_{diff} is less than R_{surf} (where L becomes sufficiently large) it starts to dominate calcite dissolution (eq 9). As the altered layer spreads out spatially and grows wider locally, the overall calcite dissolution in the fracture decreases.

During the course of the experiment, the measured Mg concentration doubled, increasing from 0.005 mol/kgw to 0.01 mol/kgw, indicating that dolomite dissolution rate increased over time. The extent of dolomite dissolution and the temporal evolution are captured by the simulation in which a diffusion limitation is included. In the simulation, the increase in the dolomite dissolution rate is a response to the decrease in calcite dissolution rate over time, which results in a lower pH increase and, thus, more rapid dolomite dissolution due to its pH dependence (eq 12).

3.3. Fracture-Aperture Change. As a result of the removal of dolomite, the fracture aperture increases. The fracture aperture map derived from the micro-CT images illustrates the localized increase (Figure 3a). In the channel, the observed aperture increase is highest at the inlet, reaching as much as 1.3 mm.[15] Similar spatial patterns are observed in the fracture aperture maps (shown as the increase in aperture versus the baseline initial aperture) generated by the simulations. The channelization is captured in both simulations regardless of the diffusion-limitation configuration (Figure 3b,c). This is because the aperture change is controlled by initial fracture geometry and dolomite dissolution, and the feedback between flow and dolomite reaction is less affected by the presence of an altered layer.

However, notable differences exist between the two simulations with and without the diffusion limitation. The aperture increase predicted in the simulation with the diffusion limitation is in general larger, with an average of 115 μm, in comparison with a 62 μm increase in the simulation without the diffusion limitation. Although the result of the simulation

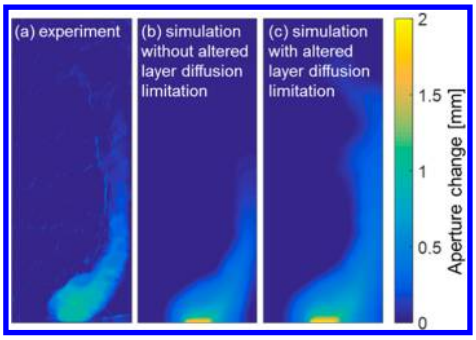

Figure 3. Color maps of fracture-aperture increase in units of mm (a) derived from the micro-CT images and generated by the 2.5D continuum model (b) without the diffusion limitation and (c) with the diffusion limitation after 113 h of reactive flow.

without the diffusion limitation is closer to the micro-CT data, which showed an increase of 65 μm in the average aperture, it evidently underestimates the extent of dolomite dissolution as indicated by the effluent measurements. As mentioned in section 3.1, there may be dissolution of dolomite in the rock matrix, which does not translate into aperture change that is captured in the micro-CT data but is included in the dolomite aperture calculation (eq 2). The other difference between the two simulations is that the channel penetrates deeper into the fracture and is more diffuse in the simulation with the diffusion limitation, agreeing more closely with the experimental observations. These differences are caused by the higher dissolution rate of dolomite (resulting from the lower solution pH values locally) and the greater overall dolomite dissolution in the simulation with the diffusion limitation.

The difference in the spatial patterns of aperture increase produced by the simulations with and without the diffusion limitation is significant despite the potential uncertainties. Variations in numerical schemes, grid resolution, and D_0 values for Ca^{2+}, Mg^{2+}, carbonate, and bicarbonate[37−39] do not result in substantial differences in the spatial patterns of fracture-aperture change (see the Supporting Information).

3.4. Altered-Layer Development. Although accurate quantification of the thickness of the altered layer from the micro-CT images is extremely challenging,[5] semiquantitative information was derived based on visual examination of the images. A thickness of approximately 0.3 mm is measured in the high-resolution tomography images of a subsample taken within the channeled fracture, and thicknesses up to ~0.5 mm were observed in the in situ micro-CT images (Figure 4).

Figure 4 maps the thickness of the altered layer (L) generated by the model simulations. Here, it is assumed that the altered layers on the two fracture surfaces are symmetric, and the reported values are for a single side of the fracture surface. In the simulation without the diffusion limitation, L is overestimated because the simulated calcite dissolution rates are too high. Close to the inlet, L is predicted to reach 4.9 mm, which is 1 order of magnitude higher than the observation. In addition, the simulated spatial pattern of the altered layer is similar to the aperture change. However, as shown in the micro-CT images (Figure 4c,e), the altered layer is more diffuse across the fracture plane. This spatial pattern is captured in the simulation with the diffusion limitation, which predicts the thickness of the altered layer to be less than 1 mm with an average value of 0.59 mm, close to the observed values.

DOI: 10.1021/acs.est.6b02184
Environ. Sci. Technol. XXXX, XXX, XXX−XXX

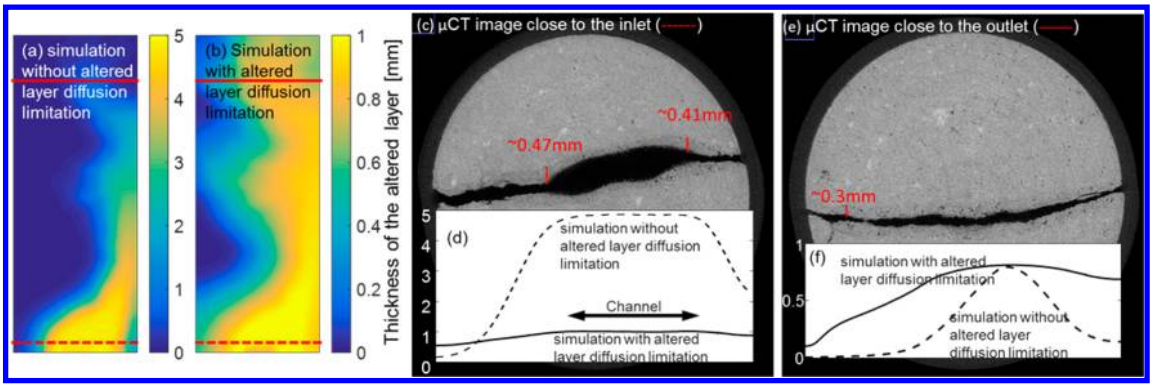

Figure 4. Thickness (mm) of the altered layer generated by the simulation (a) without and (b) with the diffusion limitation of the altered layer, (c,e) micro-CT images at the locations highlighted by the red dashed and solid lines in (a,b) illustrating the altered layer, and (d,f) the profiles of the altered-layer thickness at the same location from the simulations after 113 h of reactive flow.

In the experimental study,[15] the authors observed that close to the inlet of the core the altered layer tends to be thinner in the channel, and the thickest altered layer is located on the sides of the channel (Figure 4c). This was attributed to the fact that in the channel there is a larger supply of low-pH reactive fluid that removes both dolomite and calcite. This effect is captured by the model (Figure 4d), with the thickness of the altered layer determined by the difference between the calcite aperture and dolomite aperture, and the dolomite aperture is largest in the channel.

The simulation with the diffusion limitation overestimates L, particularly in the channel. Because the estimated effluent chemistry agrees well with the experimental measurements, the discrepancy is unlikely to be caused by the overestimation of calcite dissolution. This discrepancy may be attributed to the large uncertainties associated with the experimental measurements based on visual inspection of the micro-CT images and to the fact that similar to the dolomite aperture calculation, calcite aperture calculation include calcite dissolution that is not well-captured by the micro-CT images at the given resolution.

3.5. Other Transport Limitations across the Fracture Aperture. The diffusion-boundary layer in the fluid phase limits the overall reaction rate,[28,40] as in the case of the diffusion limitation observed in the porous altered layer. In our 2.5D continuum model, aqueous species concentrations are assumed to be well-mixed, and therefore, the impact of the diffusion boundary layer is not included. Inclusion of this effect requires discretization of the fracture aperture, as in Molins et al. (2014).[41] However, where diffusion limitation in the porous altered layer is important, the impact of the diffusion boundary layer is likely to be negligible.

The diffusion-controlled rate constants of the altered layer and the boundary layer are formulated similarly (e.g., eq 5). D_{eff} used to describe the transport limitation of the altered layer is orders of magnitude lower than D_0 that describes diffusive transport in the boundary layer,[42] and the altered layer is most likely thicker than the diffusion-boundary layer.[5,15,41−43] Therefore, the diffusion limitation caused by the altered layer will be much more important than that associated with the diffusion-boundary layer (see the Supporting Information).

3.6. Altered Layer Development at Different Flow Rates. The ability of the 2.5D continuum model to capture the development of the altered layer in fractures makes it a useful tool for investigations of different factors that affect this process. In this subsection, we present an example that demonstrates how the altered layer and its impact on overall reaction are influenced by the variations in flow rate.

In the simulations presented here, the same geometry, geochemical conditions, and transport properties (e.g., D_{eff}) of the Duperow fracture simulation were used, and the flow rate was varied between 1 and 10 μL/min (Figure 5). At the low

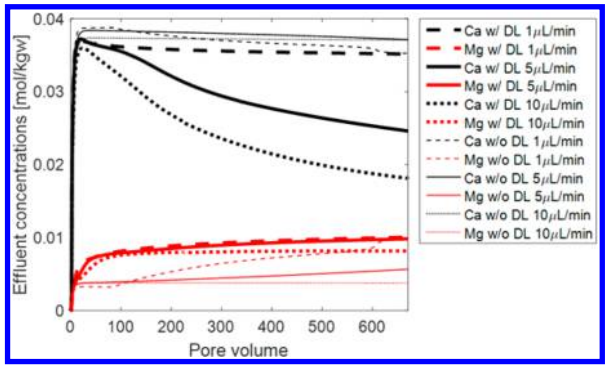

Figure 5. Effluent Ca (black) and Mg (red) concentrations from the simulations with (thick lines) and without (thin lines) the altered-layer diffusion limitation at a flow rate of 1 μL/min (--), 5 μL/min (−), and 10 μL/min (···).

flow rate, the effluent Ca concentration continues to be high, whereas at the higher flow rate, the Ca concentration in the effluent decreases dramatically. After we flooded the fracture with the same pore volume of reactive fluid, the effluent Ca concentration in the 10 μL/min simulation is reduced to half of that in the 1 μL/min simulation. These differences are not caused by the diluting effect of higher volumetric flux, as the same simulations without the diffusion limitation predict comparable effluent Ca concentrations. They are, instead, the result of the variations in the spatial patterns of the altered layer developed at different flow rates. At the low flow rate, the altered layer was limited at the inlet, and the absence of the altered layer downstream allows relatively fast calcite dissolution and maintains high Ca concentration at the outlet. In comparison, at the high flow rate, the altered layer coats most of the fracture surfaces and limits calcite dissolution throughout the fracture. Consequently, the effluent Ca concentration drops significantly as the altered layer develops.

The results have important implications for the evolution of solute transport and geochemical reaction in fractures bordered by altered layers. For example, it indicates that at higher flow

DOI: 10.1021/acs.est.6b02184
Environ. Sci. Technol. XXXX, XXX, XXX−XXX

rate, overall release of contaminants from the rock matrix into the fracture flow may be limited by diffusion through the altered layer.

4. ENVIRONMENTAL IMPLICATIONS

The novel 2.5D continuum model developed in this study tracks the reaction fronts of different minerals, updates fracture permeability accordingly, and calculates the thickness of the altered layer over time. Given these features, the model captures the spatial evolution of fracture aperture and demonstrates that the initial fracture-aperture variation and the feedback between flow and reactions in the 2D fracture plane determines the spatial pattern of the fracture evolution. In addition, it simulates the development of an altered layer as a result of preferential dissolution of the fast-reacting mineral, accounting for the influence of the altered layer on subsequent overall reaction rates of the fast-reacting mineral. The model results agree well with a previously documented experimental study, showing that as the altered layer grows, further dissolution of calcite is progressively limited. Although the input parameter D_{eff} appears to be a fitting parameter, it is a reasonable estimate based on Archie's law given the observed porosity in the altered layer.

The model provides a computationally efficient tool for further investigations of the altered layer in reactive fracture. As demonstrated in this study, at higher flow rate, the altered layer develops in a larger portion of the fracture, thus imposing a stronger limitation on overall calcite dissolution. Moreover, as the model treats the altered layer and its diffusion limitation explicitly, different reactions can be readily incorporated. One potential application of the model is to investigate to what extent precipitates on mineral surfaces may serve as a diffusion barrier and suppress further dissolution of the underlying minerals in coupled precipitation−dissolution systems, as observed in previous experimental study.[44] The model can also be used to investigate the release of contaminants from rock matrix into the fracture in the presence of an altered layer, which will provide important insights regarding the temporal profile of contamination concentrations in fractured systems that undergo such alteration. Even though the continuum model solves transient flow using Darcy's law, and therefore requires the flow regime be laminar, it should be applicable in most geological systems, where Darcy's law is valid.

The current model does not include geomechanical processes, which can be important in affecting fracture evolution.[21] However, the output of the model, including the thickness and spatial distribution of the altered layer, may be used in geomechanical models to examine fracture evolution under prevailing geomechanical stresses.

■ ASSOCIATED CONTENT

Supporting Information

The Supporting Information is available free of charge on the ACS Publications website at DOI: 10.1021/acs.est.6b02184.

Additional details including a description of the reactive transport model, image segmentation and porosity characterization, flow regime of the Duperow experiment, fluid reactivity within the fractures, and sensitivity analysis of the spatial patterns of fracture alteration to different variables. Figures showing high-resolution tomography images, porosity estimates, pH values within the fracture plane, and fracture aperture and altered-layer thickness changes. Tables showing mineral reactions included in the reactive transport modeling and aqueous complexation reactions. (PDF)

■ AUTHOR INFORMATION

Corresponding Author

*Phone: 609-937-9927; e-mail: hangdeng@lbl.gov.

Notes

The authors declare no competing financial interest.

■ ACKNOWLEDGMENTS

This work was supported as part of the Center for Nanoscale Controls on Geologic CO_2 (NCGC), an Energy Frontier Research Center funded by the U.S. Department of Energy, Office of Science, Basic Energy Sciences under award no. DE-AC02-05CH11231. Tomography experiments discussed were performed with the assistance of Dula Parkinson and Alastair MacDowell at the Advanced Light Source, Beamline 8.3.2, supported by the Office of Basic Energy Sciences, U.S. Department of Energy (contract no. DE-AC02-05CH11231).

■ REFERENCES

(1) DePaolo, D. J.; Orr, F. M., Jr. Geoscience research for our energy future. *Phys. Today* **2008**, *61* (8), 46−51.

(2) Witherspoon, P. A.; Cook, N. G. W.; Gale, J. E. Geologic Storage of Radioactive-Waste - Field Studies in Sweden. *Science* **1981**, *211* (4485), 894−900.

(3) Pruess, K. On CO(2) fluid flow and heat transfer behavior in the subsurface, following leakage from a geologic storage reservoir. *Environ. Geol.* **2008**, *54* (8), 1677−1686.

(4) Vengosh, A.; Jackson, R. B.; Warner, N.; Darrah, T. H.; Kondash, A. A Critical Review of the Risks to Water Resources from Unconventional Shale Gas Development and Hydraulic Fracturing in the United States. *Environ. Sci. Technol.* **2014**, *48* (15), 8334−8348.

(5) Noiriel, C.; Made, B.; Gouze, P. Impact of coating development on the hydraulic and transport properties in argillaceous limestone fracture. *Water Resour. Res.* **2007**, *43* (9), W09406.

(6) Ellis, B. R.; Fitts, J. P.; Bromhal, G. S.; McIntyre, D. L.; Tappero, R.; Peters, C. A. Dissolution-Driven Permeability Reduction of a Fractured Carbonate Caprock. *Environ. Eng. Sci.* **2013**, *30* (4), 187−193.

(7) Ellis, B. R.; Peters, C. A.; Fitts, J.; Bromhal, G.; McIntyre, D.; Warzinski, R.; Rosenbaum, E. Deterioration of a fractured carbonate caprock exposed to CO2-acidified brine flow. *Greenhouse Gases: Sci. Technol.* **2011**, *1* (3), 248−260.

(8) Deng, H.; Fitts, J. P.; Crandall, D.; McIntyre, D.; Peters, C. A. Alterations of Fractures in Carbonate Rocks by CO2-Acidified Brines. *Environ. Sci. Technol.* **2015**, *49* (16), 10226−10234.

(9) Elkhoury, J. E.; Ameli, P.; Detwiler, R. L. Dissolution and deformation in fractured carbonates caused by flow of CO2-rich brine under reservoir conditions. *Int. J. Greenhouse Gas Control* **2013**, *16* (1), S203−S215.

(10) Elkhoury, J. E.; Detwiler, R. L.; Ameli, P. Can a fractured caprock self-heal? *Earth Planet. Sci. Lett.* **2015**, *417*, 99−106.

(11) Andreani, M.; Gouze, P.; Luquot, L.; Jouanna, P. Changes in seal capacity of fractured claystone caprocks induced by dissolved and gaseous CO2 seepage. *Geophys. Res. Lett.* **2008**, *35* (14), L14404.

(12) Garcia-Rios, M.; Luquot, L.; Soler, J. M.; Cama, J. Influence of the flow rate on dissolution and precipitation features during percolation of CO2-rich sulfate solutions through fractured limestone samples. *Chem. Geol.* **2015**, *414*, 95−108.

(13) Singurindy, O.; Berkowitz, B. The role of fractures on coupled dissolution and precipitation patterns in carbonate rocks. *Adv. Water Resour.* **2005**, *28* (5), 507−521.

(14) Szymczak, P.; Ladd, A. J. C. Wormhole formation in dissolving fractures. *J. Geophys. Res.* **2009**, *114*, B06203.

DOI: 10.1021/acs.est.6b02184
Environ. Sci. Technol. XXXX, XXX, XXX−XXX

(15) Ajo-Franklin, J., Marco, V.; Molins, S.; Yang, L. Coupled Processes in a Fractured Reactive System: A Dolomite Dissolution Study with Relevance to GCS Caprock Integrity. In *Caprock Integrity in Geological Storage: Hydrogeochemical and Hydrogeomechanical Processes and their Impact on Storage Security*; Wiley Publishing: New York, 2016; vol. in review.
(16) Deng, H.; Ellis, B. R.; Peters, C. A.; Fitts, J. P.; Crandall, D.; Bromhal, G. S. Modifications of Carbonate Fracture Hydrodynamic Properties by CO2-Acidified Brine Flow. *Energy Fuels* **2013**, *27* (8), 4221−4231.
(17) Steefel, C. I.; DePaolo, D. J.; Lichtner, P. C. Reactive transport modeling: An essential tool and a new research approach for the Earth sciences. *Earth Planet. Sci. Lett.* **2005**, *240* (3−4), 539−558.
(18) Steefel, C. I.; Lichtner, P. C. Multicomponent reactive transport in discrete fractures: I. Controls on reaction front geometry. *J. Hydrol.* **1998**, *209* (1−4), 186−199.
(19) Steefel, C. I.; Lichtner, P. C. Diffusion and Reaction in Rock Matrix Bordering a Hyperalkaline Fluid-Filled Fracture. *Geochim. Cosmochim. Acta* **1994**, *58* (17), 3595−3612.
(20) Szymczak, P.; Ladd, A. J. C. Reactive-infiltration instabilities in rocks. Fracture dissolution. *J. Fluid Mech.* **2012**, *702*, 239−264.
(21) Yasuhara, H.; Elsworth, D. A numerical model simulating reactive transport and evolution of fracture permeability. *Int. J. Numer. Anal. Methods Geomech.* **2006**, *30* (10), 1039−1062.
(22) Chen, L.; Kang, Q.; Viswanathan, H. S.; Tao, W.-Q. Pore-scale study of dissolution-induced changes in hydrologic properties of rocks with binary minerals. *Water Resour. Res.* **2014**, *50* (12), 9343−9365.
(23) Steefel, C. I.; Appelo, C. A. J.; Arora, B.; Jacques, D.; Kalbacher, T.; Kolditz, O.; Lagneau, V.; Lichtner, P. C.; Mayer, K. U.; Meeussen, J. C. L.; Molins, S.; Moulton, D.; Shao, H.; Simunek, J.; Spycher, N.; Yabusaki, S. B.; Yeh, G. T. Reactive transport codes for subsurface environmental simulation. *Computational Geosciences* **2015**, *19* (3), 445−478.
(24) Pruess, K.; Wang, J. S. Y.; Tsang, Y. W. on Thermohydrologic Conditions near High-Level Nuclear Wastes Emplaced in Partially Saturated Fractured Tuff 0.1. Simulation Studies with Explicit Consideration of Fracture Effects. *Water Resour. Res.* **1990**, *26* (6), 1235−1248.
(25) Smith, L. Flow and Reactions in Permeable Rocks - Phillips,Om. *Science* **1991**, *253* (5026), 1430−1430.
(26) Steefel, C. I.; Lasaga, A. C. a Coupled Model for Transport of Multiple Chemical-Species and Kinetic Precipitation Dissolution Reactions with Application to Reactive Flow in Single-Phase Hydrothermal Systems. *Am. J. Sci.* **1994**, *294* (5), 529−592.
(27) Lasaga, A. C. Metamorphic Reaction-Rate Laws And Development Of Isograds. *Mineral. Mag.* **1986**, *50* (357), 359−373.
(28) Casey, W. H. Heterogeneous Kinetics and Diffusion Boundary-Layers - the Example of Reaction in a Fracture. *J. Geophys. Res.* **1987**, *92* (B8), 8007−8013.
(29) Rickard, D.; Sjoberg, E. L. Mixed Kinetic Control of Calcite Dissolution Rates. *Am. J. Sci.* **1983**, *283* (8), 815−830.
(30) Nicholson, R. V.; Gillham, R. W.; Reardon, E. J. Pyrite Oxidation in Carbonate-Buffered Solution 0.2. Rate Control by Oxide Coatings. *Geochim. Cosmochim. Acta* **1990**, *54* (2), 395−402.
(31) Mayer, K. U.; Frind, E. O.; Blowes, D. W. Multicomponent reactive transport modeling in variably saturated porous media using a generalized formulation for kinetically controlled reactions. *Water Resour. Res.* **2002**, *38* (9), 13-1.
(32) Murphy, W. M.; Oelkers, E. H.; Lichtner, P. C. Surface-Reaction versus Diffusion Control of Mineral Dissolution and Growth-Rates in Geochemical Processes. *Chem. Geol.* **1989**, *78* (3−4), 357−380.
(33) Steefel, C. I.; Maher, K. Fluid-Rock Interaction: A Reactive Transport Approach. In *Thermodynamics and Kinetics of Water-Rock Interaction*; Oelkers, E. H., Schott, J., Eds.; Mineralogical Society of America: Chantilly, VA, **2009**; Vol. *70*, pp 485−532.
(34) Sjoberg, E. L.; Rickard, D. T. Temperature-Dependence of Calcite Dissolution Kinetics between 1-Degree-C and 62-Degrees-C at Ph 2.7 to 8.4 in Aqueous-Solutions. *Geochim. Cosmochim. Acta* **1984**, *48* (3), 485−493.
(35) Pokrovsky, O. S.; Golubev, S. V.; Schott, J. Dissolution kinetics of calcite, dolomite and magnesite at 25 degrees C and 0 to 50 atm pCO(2). *Chem. Geol.* **2005**, *217* (3−4), 239−255.
(36) Azar, J. H.; Javaherian, A.; Pishvaie, M. R.; Nabi-Bidhendi, M. An approach to defining tortuosity and cementation factor in carbonate reservoir rocks. *J. Pet. Sci. Eng.* **2008**, *60* (2), 125−131.
(37) Oelkers, E. H.; Helgeson, H. C. Calculation of the Thermodynamic and Transport-Properties of Aqueous Species at High-Pressures and Temperatures - Aqueous Tracer Diffusion-Coefficients of Ions to 1000-Degrees-C and 5-Kb. *Geochim. Cosmochim. Acta* **1988**, *52* (1), 63−85.
(38) Yuan-Hui, L.; Gregory, S. Diffusion of Ions in Sea-Water and in Deep-Sea Sediments. *Geochim. Cosmochim. Acta* **1974**, *38* (5), 703−714.
(39) Rard, J. A.; Miller, D. G. Mutual Diffusion-Coefficients of NaCl-H_2O and $CaCl_2$-H_2O at 25-Degrees-C from Rayleigh Interferometry. *J. Solution Chem.* **1979**, *8* (10), 701−716.
(40) Noiriel, C.; Steefel, C. I.; Yang, L.; Ajo-Franklin, J. Upscaling calcium carbonate precipitation rates from pore to continuum scale. *Chem. Geol.* **2012**, *318-319*, 60−74.
(41) Molins, S.; Trebotich, D.; Yang, L.; Ajo-Franklin, J. B.; Ligocki, T. J.; Shen, C.; Steefel, C. I. Pore-Scale Controls on Calcite Dissolution Rates from Flow-through Laboratory and Numerical Experiments. *Environ. Sci. Technol.* **2014**, *48* (13), 7453−7460.
(42) Bradbury, M. H.; Green, A. Investigations into the Factors Influencing Long-Range Matrix Diffusion Rates and Pore-Space Accessibility at Depth in Granite. *J. Hydrol.* **1986**, *89* (1−2), 123−139.
(43) De Baere, B.; Molins, S.; Mayer, K. U.; François, R. Determination of mineral dissolution regimes using flow-through time-resolved analysis (FT-TRA) and numerical simulation. *Chem. Geol.* **2016**, *430*, 1−12.
(44) Singurindy, O.; Berkowitz, B. Evolution of hydraulic conductivity by precipitation and dissolution in carbonate rock. *Water Resour. Res.* **2003**, *39* (1), 14.

DOI: 10.1021/acs.est.6b02184
Environ. Sci. Technol. XXXX, XXX, XXX−XXX